Supporting Information

for

Construction of N-doped nickel sulfide nanosheets via PANI as Nitrogen donor for superior electrocatalytic water splitting

Liwen Hu, [1,2*] *Dan Xiang,* [1,2] *Yi Gan,* [1,2] *LiangYing Wen,*[1,2] *Xuewei Lv,* [1,2] *Meilong Hu,* [1,2] *Yuntao Xin,* [1,2] *Zhuoran Hou* [1,2*]

[1]*College of Materials Science and Engineering, Chongqing University, Chongqing 400044, PR China*

[2]*Chongqing Key Laboratory of Vanadium-Titanium Metallurgy and New Materials, Chongqing University, Chongqing 400044, PR China*

***Corresponding author:** Liwen Hu, Zhuoran Hou

E-mail: lwh0423@cqu.edu.cn, 851496419@qq.com

Phone: +86-23-65112631;

Address: College of Materials Science and Engineering, Chongqing University, Chongqing 400044, PR China

1. Materials Characterizations

In order to analyze the phase composition, crystal structure and morphology of the samples, the samples were detected by X-ray diffraction (XRD, D/MAX 2500 PC), scanning electron microscope (SEM, Fei Quattro s), transmission electron microscope (TEM, FEI Talos F200S) and X-ray photoelectron spectroscopy (XPS, Thermo Scientific K-Alpha).

2. Electrochemical measurements

The electrochemical tests described in this paper were all carried out using CHI660E workstation (Shanghai Instrument Co., Ltd.). In the test process, the nickel foam electrode, the graphite rod and the saturated calomel electrode (SCE) made up a three-electrode system. And electrochemical impedance spectroscopy (EIS) was measured in a frequency range of 0.01Hz to 100 kHz with an amplitude of 0.01 V. In the HER process, the linear sweep curve (LSV) and the Tafel curve were measured at a sweep rate of 2 mV/s and 0.1 mV/s, respectively. The double layer capacitance (C_{DL}) was measured at different scan rates in the non-faraday region (CV) using cyclic voltammetry. The cyclic stability of the sample was calculated after 24 h operation at 10 mA/cm^2. The polarization curve was calibrated by ohmic potential drop, and all electrochemical test potentials were corrected by resistance compensation and converted to RHE according to the following formula:

$E_{RHE} = E_{appl} + E_{SCE} + 0.0592pH \approx E_{appl} + 1.07$

3. Density Functional Theory (DFT) Calculations

To understand the mechanism of increased HER activity in MCG in alkaline environments, density functional theory (DFT) calculations were performed using the Vienna AB Initio Simulation Package (VASP). The energy associated with electron exchange is described by a generalized gradient approximation (GGA) with a Perdew Burke Ernzerhof (PBE) function. In the calculation, the Monkhorst-Pack K grid in the

Brillouin region is set as a 3 × 2 × 1 grid centered on the Gamma point. Throughout the calculation, the cutoff energy was set to 500 eV. The standard settings for electronic structure iterations are 1×10^{-5} eV and 0.001 eV $Å^{-1}$.

In this work, a (1 1 0) cross-section of the crystal structure was performed. An axial vacuum of 15 Å is then used, which is sufficient to avoid image interactions. The adsorption energy (ΔE(eV)) of the H atom on the substrate is defined as:

$\Delta E = E_{*H} - (E^* + E_H)$

where E*H(eV) and E* represent the energy of the substrate with H atom adsorbed and the energy of the pure substrate, respectively, and the energy of EH refers to the energy of one hydrogen atom. The standard Gibbs free energy change (ΔG (eV)) can be calculated as:

$\Delta G = \Delta E + (\Delta ZPE - T\Delta S)$

where E (eV) is the binding energy and ZPE (eV) is the zero-point energy. Both of them can be calculated by DFT. S represents entropy, and the value of TΔS is obtained by calculation.

4. Calculation of the turnover frequency (TOF)

The turnover frequencies were calculated with the following equation：

$$TOF = \frac{I\ 1}{Fn2}$$

Here, I and F represent the current (A) during the linear sweep measurement and faraday constant (C/mol), and n represents the number of active sites (mol). The factor 1/2 arrives by taking into account that two electrons are required to form one hydrogen molecule from two protons. We tested CV curve in the region of -0.2 to 0.6 V vs. RHE (50 mV/s) of N-NiS@NF in 1 M KOH solution. The integral charge over the entire potential range should be proportional to the total number of active sites. Assuming that both reduction and oxidation processes are single electron processes, the upper limit of active sites can be calculated.

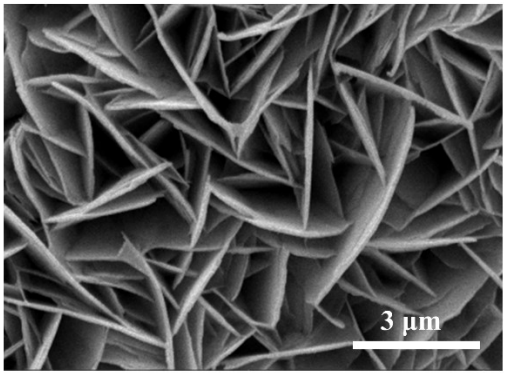

Fig. S1 SEM image of $Ni(OH)_2$.

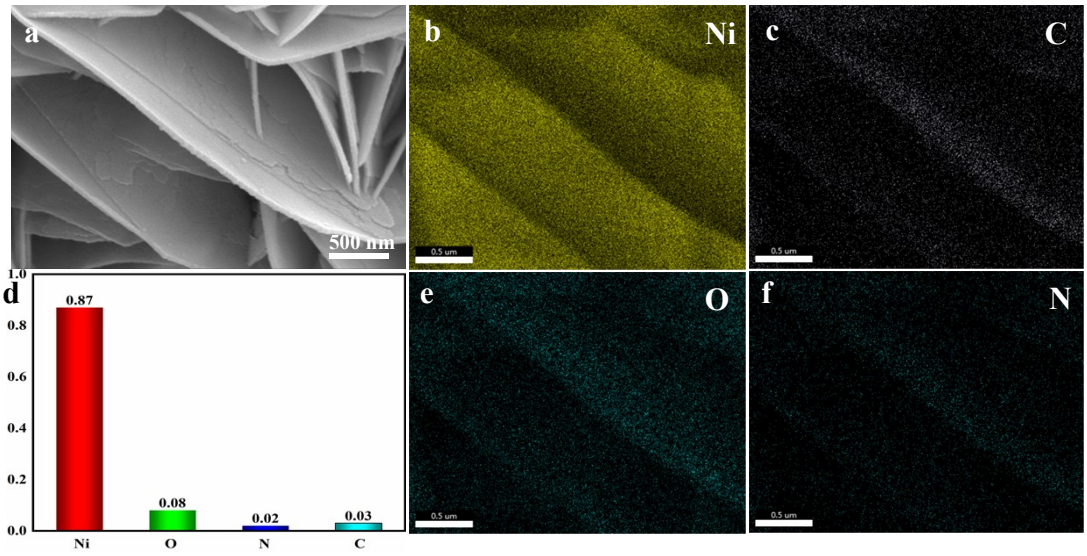

Fig. S2 (a) **SEM** image of PANI-Ni(OH)$_2$, (b, c, e, f) **EDS** spectra of Ni, C, O, N respectively, (d) Content ratio of each element in PANI-Ni(OH)$_2$.

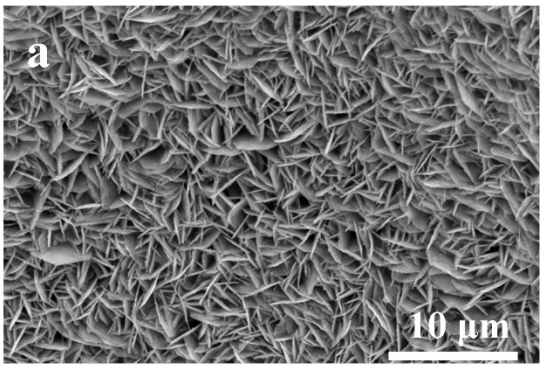

Fig. S3 (a) **SEM** image of NiS.

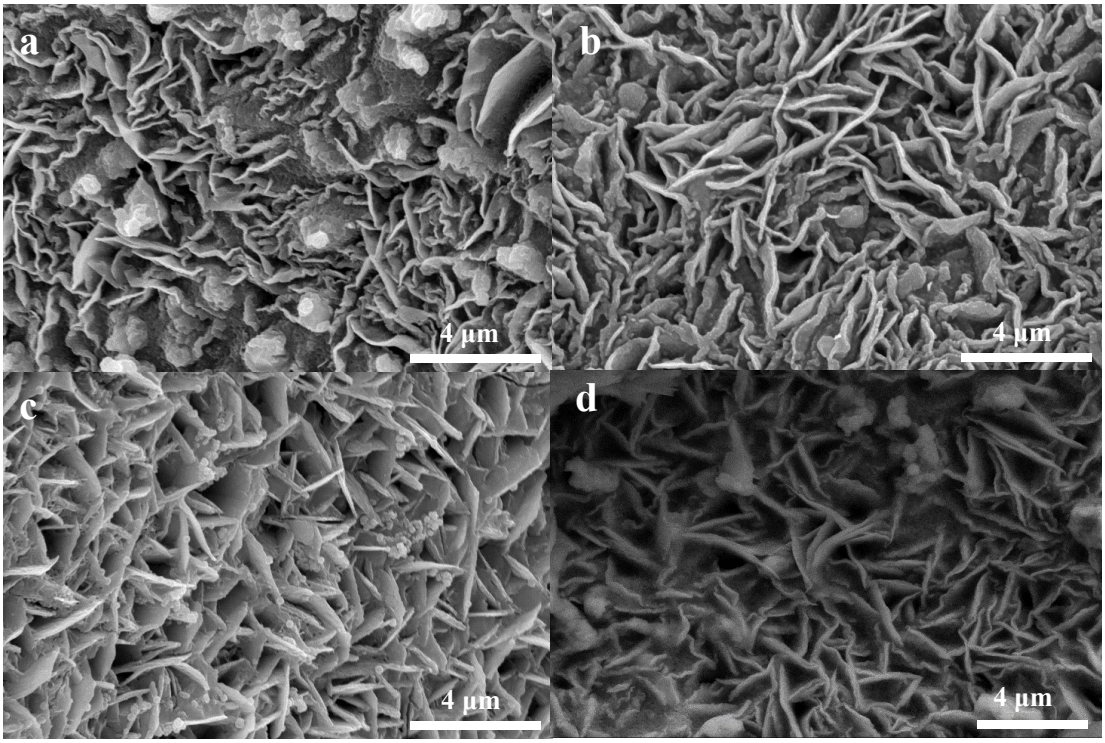

Fig. S4 (a) SEM image of N-NiS-1, (b) SEM image of N-NiS-2, (c) SEM image of N-NiS-3, (d) SEM image of N-NiS-4.

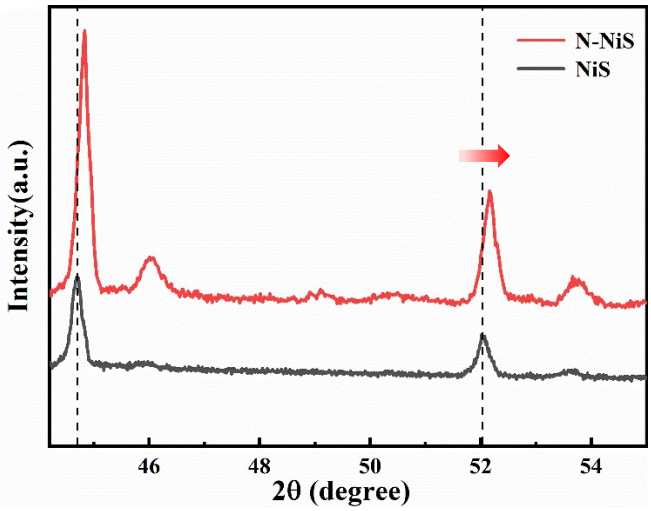

Fig. S5 Local **XRD** patterns of NiS and N-NiS.

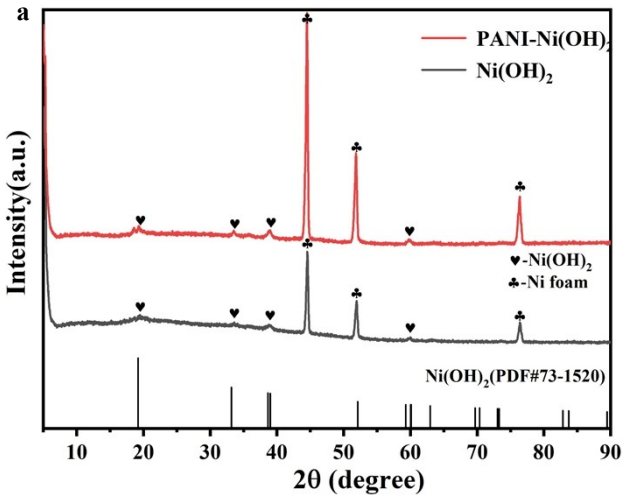

Fig. S6 XRD patterns of $Ni(OH)_2$ and PANI- $Ni(OH)_2$.

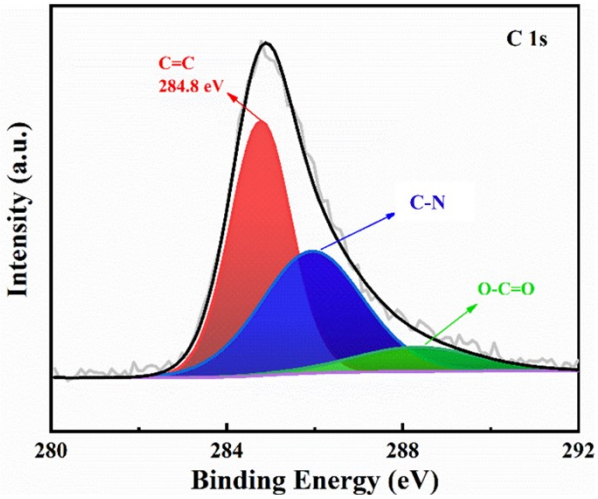

Fig. S7 XPS measurement spectrum of C 1s.

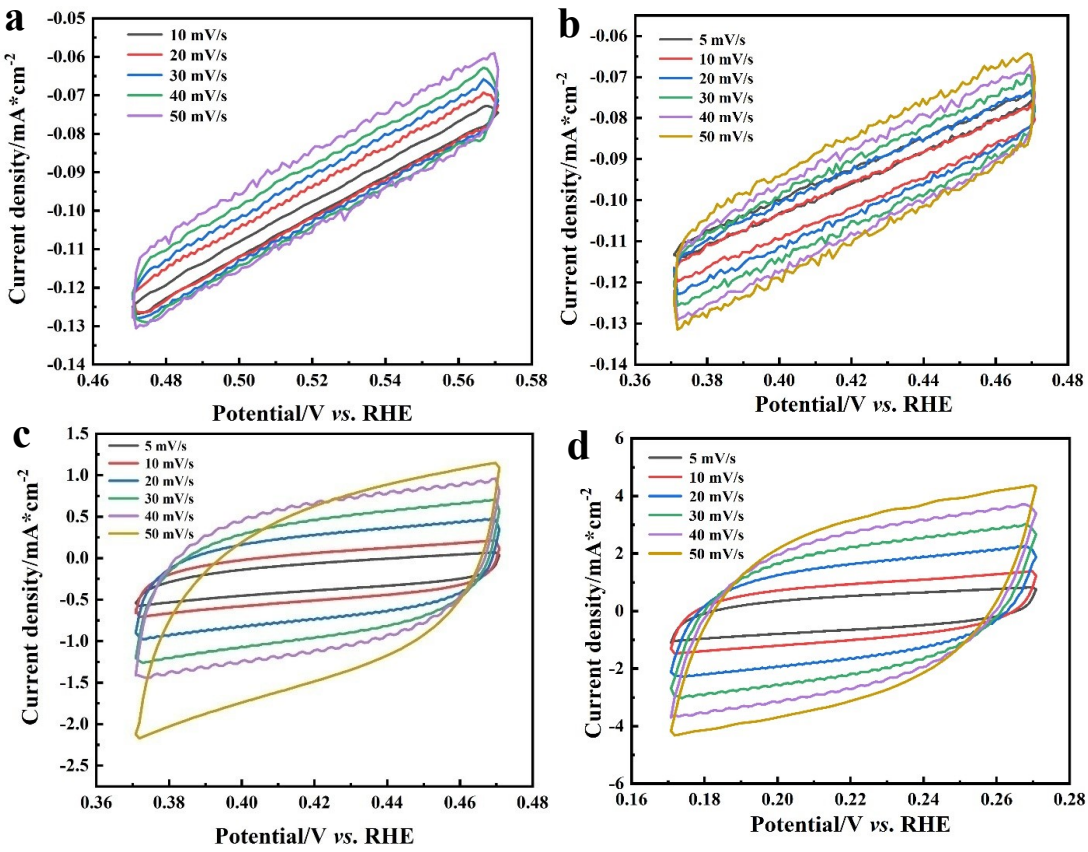

Fig. S8 Cyclic voltammetry (CV) curves of (a) $Ni(OH)_2$, (b) PANI-$Ni(OH)_2$, (c) NiS, (d) N-NiS.

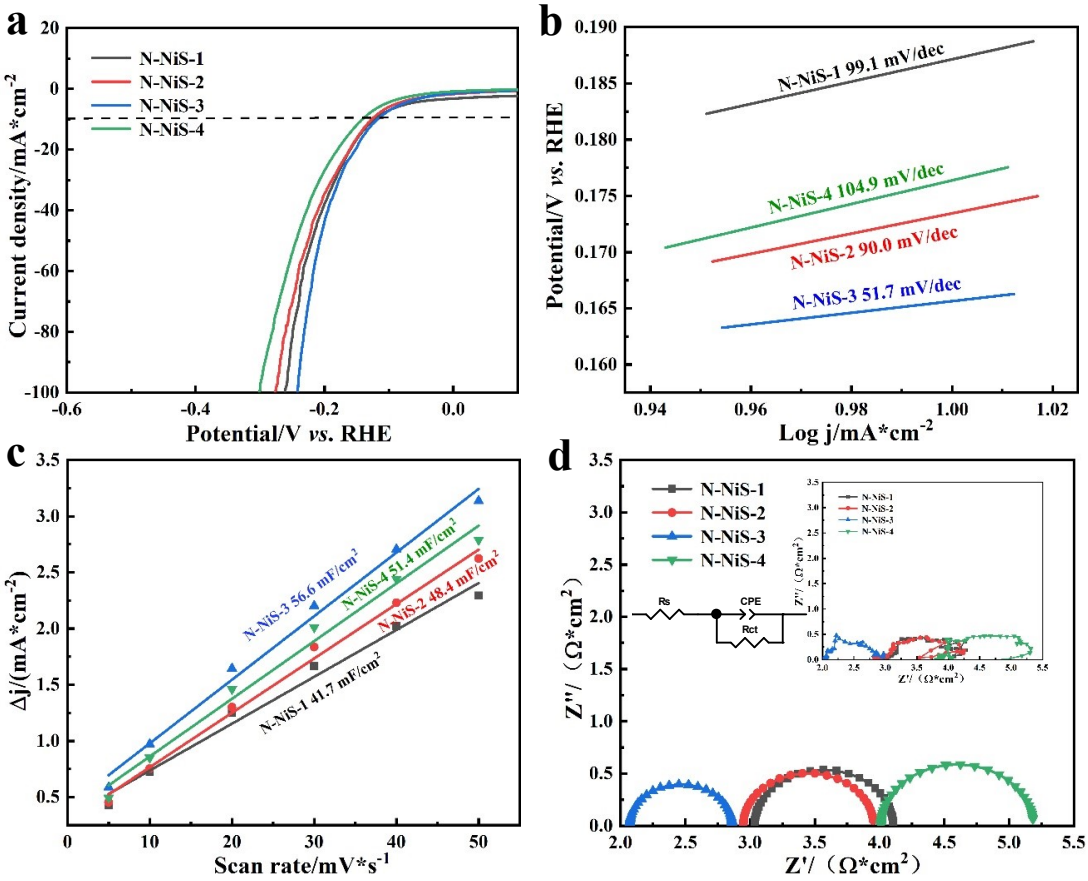

Fig. S9 (a) LSV diagrams of N-NiS with different coating contents, (b) Tafel plots of N-NiS with different coating contents, (c) C_{dl} of N-NiS with different coating contents (d) Summary of impedance spectra of N-NiS with different coating contents.

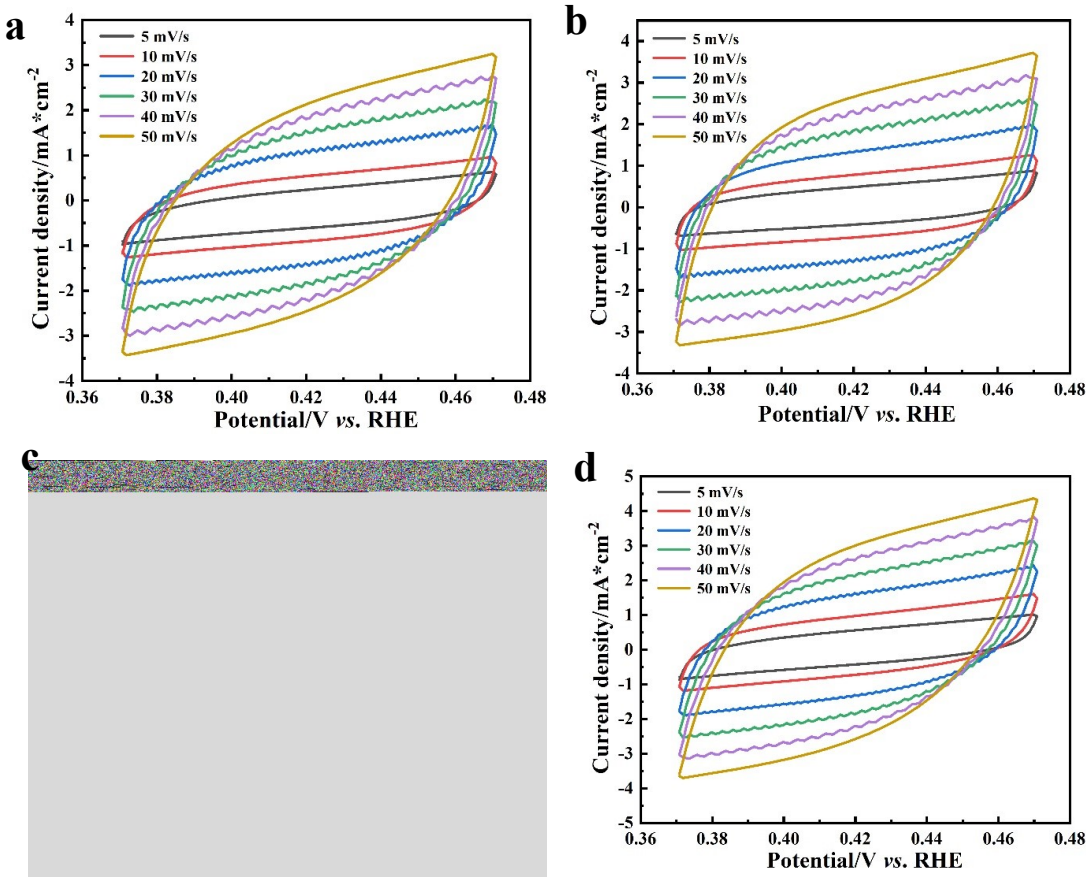

Fig. S10 Cyclic voltammetry (CV) curves of (a) N-NiS-1, (b) N-NiS-2, (c) N-NiS-3, (d) N-NiS-4 in the Faraday region.

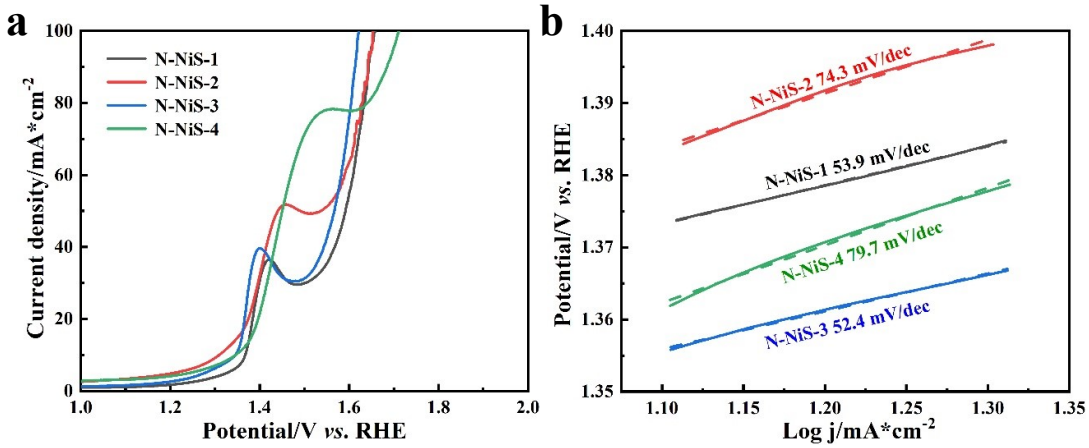

Fig. S11 (a) LSV diagrams of N-NiS with different coating contents, (b) Tafel plots of N-NiS with different coating contents.

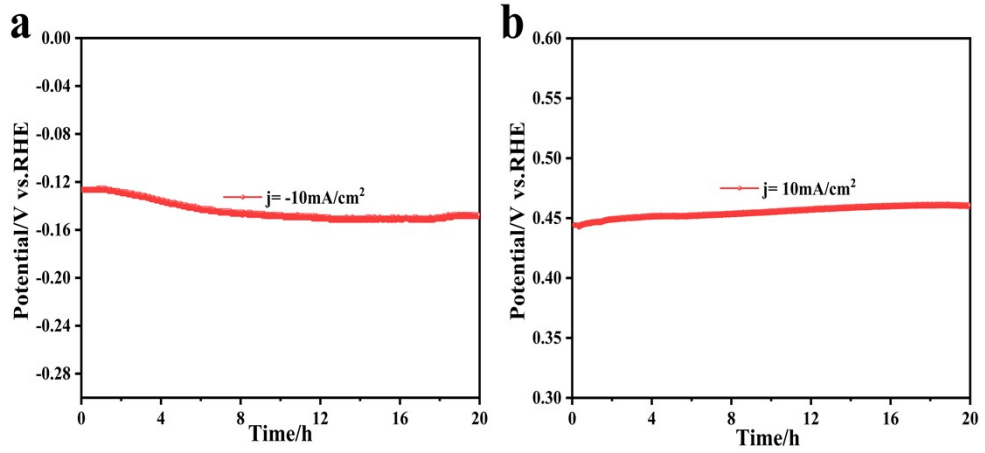

Fig.S12 I–t chronoamperometric curve of N-NiS in 1.0 M KOH at 10 mA/cm^2 for 20h respectively both HER (a) and OER (b).

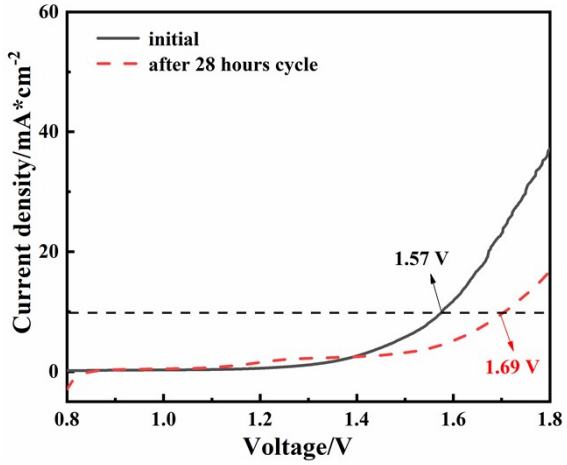

Fig.S13 LSV curves of N-NiS/NFs ‖ N-NiS/NFs before and after the cycling stability test for 28h.

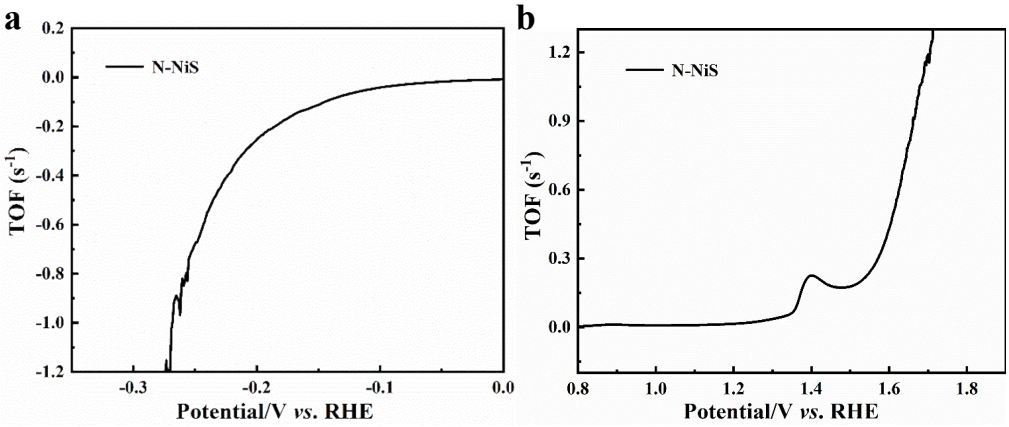

Fig.S14 (a) The calculated turnover frequency curve of N-NiS@NF catalyst for HER, (b) The calculated turnover frequency curve of N-NiS@NF catalyst for OER. The TOF value for HER at -100 mV is -0.10 s^{-1}. And the TOF value for OER at 300 mV is 0.22 s^{-1}.

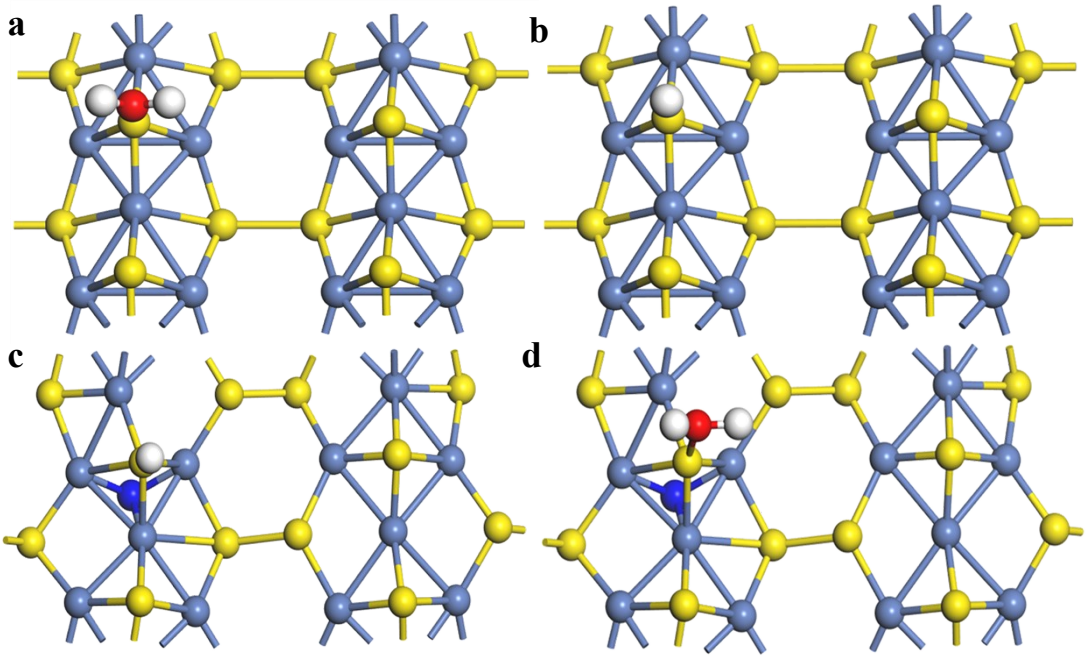

Fig. S15 (a) Schematic diagram of NiS water adsorption, (b) Schematic diagram of NiS hydrogen adsorption, (c) Schematic diagram of N-NiS hydrogen adsorption, (a) Schematic diagram of N-NiS water adsorption.

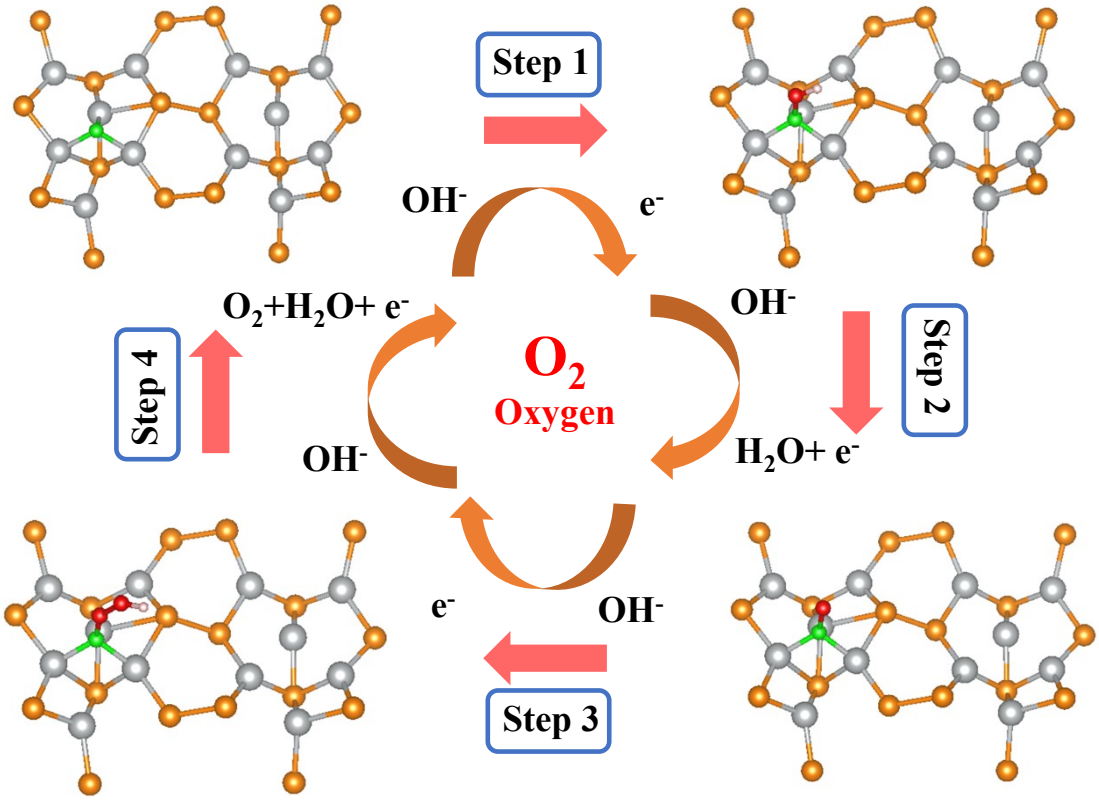

Fig. S16 OER mechanism diagram.

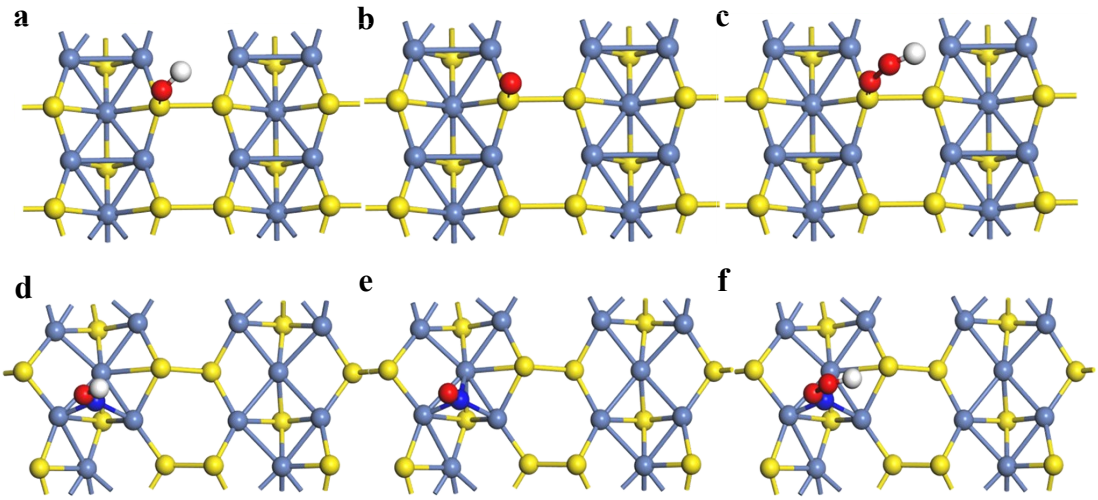

Fig. S17 (a) Schematic diagram of NiS *OH adsorption, (b) Schematic diagram of NiS *O adsorption, (c) Schematic diagram of NiS *OOH adsorption, (d) Schematic diagram of N-NiS *OH adsorption, (e) Schematic diagram of N-NiS *O adsorption, (f) Schematic diagram of N-NiS *OOH adsorption.

Table. S1 Comparison of **HER** performance between N-NiS and other non-precious metal bifunctional electrocatalysts in 1.0 M KOH.

Catalyst type	Current density (mA/cm^2)	Overpotential (mV)	Tafel slope (mV/dec)	Ref.
N-NiS	10	117	64.8	This work
NiS_2	10	174	63	[1]
$MoS_2/NiSeNi_3S_2$	10	181	70.0	[2]
$Ni_xCo_{3-x}S_4/Ni_3S_2/NF$	10	258	107	[3]
$NiCo_2S_4/Ni_3S_2/NF$	10	119	105.2	[4]
DE-TDAP	10	154	83	[5]
N, S Co-carbon tubes	10	280	126	[6]
CoMoP@N, P-C	10	152	76.8	[7]
CoMo@CN	10	218	73.5	[8]
3D-rGO-CeO_2	10	192	112.8	[9]
$Zn_{0.975}Co_{0.025}S/CoS_2$	10	152	103	[10]
Co_2B	10	233	92.5	[11]

Table. S2 Comparison of **OER** performance between N-NiS and other non-precious metal bifunctional electrocatalysts in 1.0 M KOH

Catalyst type	Current density (mA/cm^2)	Overpotential (mV)	Tafel slope (mV/dec)	Ref.
N-NiS	50	330	46.7	This work

CoMnON/N-rGO	10	350	70	[12]
NiS/Ni foam	50	335	89	[13]
CoSe/Ti mesh	50	341	69	[14]
IrO_2	10	350	67	[15]
Ni_3S_4/NF	20	320	-	[16]
NiCoS-3	10	320	58.8	[17]

Table. S3 Comparison of overall water splitting between N-NiS and other non-precious metal bifunctional electrocatalysts in 1.0 M KOH.

Catalyst type	Current density (mA/cm^2)	Cell voltage (V)	Ref.
N-NiS	10	1.57	This work
Ni_5P_4	10	1.70	[18]
N-NiCoP/NCF	10	1.56	[19]
Ni/Ni_8P_3	10	1.61	[20]
$FeNi_3N$/NF	10	1.62	[21]
$CoNi_2Se_4$	10	1.61	[22]
CoS_x/Ni_3S_2@NF	10	1.58	[23]
Co_9S_8-Ni_3S_2-CNTs/NF	10	1.65	[24]
Co_4S_3-WS_2	10	1.59	[25]
Ir-VG	10	1.57	[26]
$FeCo/Co_2P$	10	1.68	[27]
RuO_2/Co_3O_4-RuCo@NC	10	1.66	[28]

Reference

[1] P. Luo, H. Zhang, L. Liu, Y. Zhang, J. Deng, C. Xu, et al., ACS Appl. Mater. Interfaces, 2017, 9, 2500-8.

[2] Y. Guan, H. Xuan, H. Li, P. Han, Electrochim Acta, 2019, 320.

[3] Y. Wu, Y. Liu, G.-D. Li, X. Zou, X. Lian, D. Wang, et al., Nano Energy, 2017, 35, 161-70.

[4] H. Liu, X. Ma, Y. Rao, Y. Liu, J. Liu, L. Wang, et al., ACS Appl. Mater. Interfaces, 2018, 10, 10890-7.

[5] G.Yasin, S. Ibraheem, S. Ali, M. Arif, S. Ibrahim, R. Iqbal, et al., Mater. Today Chem., 2022, 23, 100634.

[6] T. Sun, Q. Wu, Y. Jiang, Z. Zhang, L. Du, L. Yang, et al., Chem. Eur. J., 2016, 22, 10326-9.

[7] Sun D, Lin S, Yu Y, Liu S, Meng F, Du G, et al. J Alloys Comp 2022;895:162595.

[8] J. Jiang, Q. Liu, C. Zeng, L. Ai, J. Mater. Chem. A, 2017, 5, 16929-35.

[9] M. Liu, Z. Ji, X. Shen, H. Zhou, J. Zhu, X. Xie, C. Song, X. Miao, L. Kong, G. Zhu, Eur. J. Inorg. Chem., 2018, 22, 3952-3959.

[10] Z. Yu, Y. Bai, S. Zhang, Y. Liu, N. Zhang, K. Sun, J. Mater. Chem., 2018, 6, 10441-10446.

[11] J. Masa, P. Weide, D. Peeters, I. Sinev, W. Xia, Z. Sun, C. Somsen, M. Muhler, W. Schuhmann, Adv. Energy Mater., 2016, 6, 1502313.

[12] Z. Yan, H. Qi, X. Bai, K. Huang, Y.-R. Chen, Q. Wang, Electrochim Acta, 2018,

283, 548-59.

[13] W. Zhu, X. Yue, W. Zhang, S. Yu, Y. Zhang, J. Wang, et al., 2016, 52, 1486-9.

[14] T. Liu, Q. Liu, A.-M. Asiri, Y. Luo, X. Sun, Chem. Commun. (Camb) 2015, 51, 16683-6.

[15] Q. Xiao, Y. Zhang, X. Guo, L. Jing, Z. Yang, Y. Xue, et al., Chem. Commun. (Camb), 2014, 50, 13019-22.

[16] J.-T. Ren, Z.-Y. Yuan, ACS Sustainable Chem. Eng. 2017, 5, 7203-10.

[17] Z. Yu, Y. Bai, S. Zhang, Y. Liu, N. Zhang, K. Sun, Inter. J. Hydrogen Energy, 2018, 43, 8815-23.

[18] M. Ledendecker, S. Krick Calderón, C. Papp, H.-P. Steinrück, M. Antonietti, M. Shalom, Angew. Chem. Inter. Ed., 2015, 54, 12361-5.

[19] R. Zhang, J. Huang, G. Chen, W. Chen, C. Song, C. Li, et al., Appl. Catal. B., 2019, 254, 414-23.

[20] G.-F. Chen, T.-Y. Ma, Z.-Q. Liu, N. Li, Y.-Z. Su, K. Davey, et al., Adv. Funct. Mater. 2016, 26, 3314-23.

[21] B. Zhang, C. Xiao, S. Xie, J. Liang, X. Chen, Y. Tang, Chem. Mater. 2016, 28, 6934-41.

[22] B.-G. Amin, A.-T. Swesi, J. Masud, M. Nath, Chem. Commun. (Camb) 2017, 53, 5412-5.

[23] S. Shit, S. Chhetri, W. Jang, N.-C. Murmu, H. Koo, P. Samanta, et al., ACS Appl. Mater. Interfaces, 2018, 10, 27712-22.

[24] Y. Yao, J. He, L. Ma, J. Wang, L. Peng, X. Zhu, et al., J. Colloid Interface Sci.,

2022, 616, 287-97.

[25] Q. Peng, X. Shao, C. Hu, Z. Luo, I.-T. Taylor, Z. Dou, et al., J. Colloid Interface Sci., 2022, 615, 577-86.

[26] S.-B. Roy, K. Akbar, J.-H. Jeon, S.-K. Jerng, L. Truong, K. Kim, Y. Yi, S.-H. Chun, J. Mater. Chem. A, 2019,7, 20590-20596.

[27] Z. Fan, J. Jiang, L. Ai, Z. Shao, S. Liu, ACS Appl. Mater. Interfaces, 2019, 11, 47894-47903.

[28] Q. Shi, Q. Liu, Y. Ma, Z. Fang, Z. Liang, G. Shao, B. Tang, W.-Y. Yang, L. Qin, X.-S. Fang, Adv. Energy Mater., 2020, 10, 1903854.